LANGMUIR

pubs.acs.org/Langmuir Article

Mechanical Properties Determination of DMPC, DPPC, DSPC, and HSPC Solid-Ordered Bilayers

Dominik Drabik,* Grzegorz Chodaczek, Sebastian Kraszewski, and Marek Langner

Cite This: *Langmuir* 2020, 36, 3826−3835 Read Online

ACCESS | Metrics & More | Article Recommendations | Supporting Information

ABSTRACT: Lipid bilayers are active participants in many crucial biological processes. They can be observed in different phases, liquid and solid, respectively. The liquid phase is predominant in biological systems. The solid phase, both crystalline and gel phases, is under investigation due to its resilience to mechanical stress and tight packing of lipids. The mechanical properties of lipids affect their dynamics, therefore influencing the transformation of cell plasma and the endomembrane. Mechanical properties of lipid bilayers are also an important parameter in the design and production of supramolecular lipid-based drug delivery systems. To this end, in this work, we focused on investigating the effect of solid phases of lipid bilayers on their structural parameters and mechanical properties using theoretical molecular dynamics studies on atomistic models of whole vesicles. Those include area per lipid, membrane thickness, density vesicle profiles, bending rigidity coefficient, and area compressibility. Additionally, the bending rigidity coefficient was measured using the flicker noise spectroscopy. The two approaches produced very similar and consistent results. We showed that, contrary to our expectations, bending rigidity coefficients of solid-ordered bilayers for vesicles decreased with an increase in lipid transition temperature. This tendency was reverse in planar systems. Additionally, we have observed an increase of membrane thickness and area compressibility and a decrease of area per lipid. We hope these results will provide valuable mechanical insight for the behavior in solid phases and differences between spherical and planar confirmations.

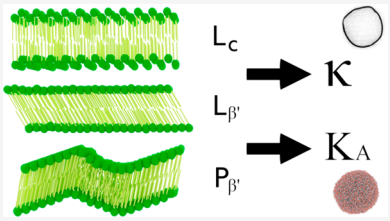

INTRODUCTION

Over past few years, lipids have been acknowledged as diverse active participants in many biological processes rather than being simple building blocks of cells components.[1] Lipids and their aggregates, apart from their barrier function, participate in metabolic processes, cytoplasm compartmentalization, and the formation of a dynamic infrastructure for the rearrangement of aqueous compartments. In the fluid mosaic membrane model, disordered bilayers are built by freely moving lipids subject to lateral diffusion. While the model is an effective tool for understanding molecular-level processes, it is unable to rationalize lipid bilayer properties. This is especially relevant in cell physiology, where the occurrence of local defects, the size, and both mechanical and electrostatic properties are necessary for ensuring local molecular homeostasis.[2] The other important feature of the biological membrane is its heterogeneity with respect to lipid composition and physicochemical properties. This gave rise to the membrane raft concept, also sometimes referred to as microdomains. They differ from the surrounding lipid matrix with respect to lipid composition and molecular packing.[3] Furthermore, individual lipid mobility and collective lipid dynamics (i.e., the packing structure and organization) depend on the activity of the surrounding water.[4] The effect of microdomains on the mechanical properties has not been thoroughly investigated.[5] The mechanics of heterogeneous lipid bilayers can be simplified by the investigation of homogeneous lipid bilayers with different lipid dynamics and different hydrocarbon chain lengths. Typically, there are four states in which the bilayer can be in the crystalline phase, gel phase (together referred to as solid phase), ripple phase, and liquid phase. When the cell membrane is fully hydrated, it is predominantly in the liquid phase. However, it transitions into the gel phase with a reduction in temperature below the so-called main transition temperature (T_m).[6]

The gel phase is mostly observed in long and saturated fatty acid chains. In that phase, the lipid head groups are very tightly packed; the lipid acyl chains become straighter and ordered, and the bilayer thickness increases.[7] The lipid bilayer formed from lipids, whose phase is well-defined at a specific temperature, is a convenient experimental model. For instance, the coexistence of gel and fluid phases has been demonstrated on membranes formed from the mixture of lipids with different T_m's. Such cases were reported for DMPC (1,2-dimyristoyl-*sn*-glycero-3-phosphocholine)−DSPC (1,2-distearoyl-*sn*-glycero-3-phosphocholine), 20:0 DMPC−PC (phosphocholine), and DMPC−DPPC (1,2-dipalmitoyl-*sn*-glycero-3-phosphocholine) mixtures using quick-freeze differential scanning calorimetry[8]

Received: February 19, 2020
Revised: March 10, 2020
Published: March 16, 2020

https://dx.doi.org/10.1021/acs.langmuir.0c00475
Langmuir 2020, 36, 3826−3835

as well as for different two-component mixtures of DSPC, DLPC, DMPC, or DAPC using model simulations.[9] From a biological perspective, the membrane is formed from lipids that are mostly unsaturated, and organisms adapt their fatty acid composition to the environment to prevent the formation of solid phases. Despite detecting solid phases in very specific cases of biological membranes like the myelin sheath or stratum corneum,[10] where it is required to form a mechanically resistant lipid barrier, it is generally considered that they do not occur in biological membranes.[11] The lipid bilayer mechanics is also a very significant property for the design of the targeted delivery system. It has been demonstrated that endocytosis depends on the nanoparticle stiffness and shape.[12] The drug carrier mechanics is also important for its stability in serum, specifically by protecting it from undesired interactions such as the interaction with lipoproteins (which are known to interact with lipids and to induce structural changes) and/or blood key proteins.[13]

In this Article, we have focused on mechanical properties of solid phase bilayers as a means to provide information about their behavior. From a general mechanical point of view, lipid systems possess a peculiar combination of elastic properties. The stretching elasticity of the lipid bilayer is described by the area compressibility modulus (K_A; N/m). It is understood that energy is necessary to stretch the bilayer into a direction perpendicular to the bilayer itself. The shear elasticity of the lipid bilayer is understood as the shear between individual lipid molecules. It is negligible in liquid-ordered phases but significant for crystallized membranes. However, the ability to bend under very low stress, the bending elasticity, is perhaps the most interesting one of the mechanical properties.[14] This ability is described by bending elasticity, κ. It is very challenging to measure this parameter as its value is very small (on the order of 10^{-19}–10^{-20} J). Due to the pioneering work of Helfrich,[15] the membrane thermal flickering phenomenon was initially observed in red blood cell membranes.[16] This discovery sparked a significant number of studies involving membrane mechanics and allowed for different approaches to determine the bending elasticity in membrane systems.[5] In this work, we have used two different techniques to determine the mechanical properties of the investigated bilayers. These bilayers consist of lipids with T_m higher than the ambient temperature often used in experimental measurements. We selected four such lipids: DMPC, DPPC, DSPC, and an HSPC (L-α-phosphatidylcholine, mixture of 11.4% DPPC and 88.6% DSPC) mixture. The measuring temperature in the experiments and simulations was selected at 295 K (22 °C). As a result, each of the investigated bilayers are measured in different solid phases. The DMPC bilayer is only 2 K below the transition temperature (T_m = 297 K) but, at the same time, higher than both subtransition and pretransition temperatures (287 and 289 K, respectively), which results in a rippled $P_{\beta'}$ gel phase. In the rippled phase, the regions in the gel phases are separated by liquid phases.[17] The DPPC bilayer is measured below its transition and pretransition temperatures (314 and 307 K, respectively) but higher than its subtransition temperature (294 K), which results in the $L_{\beta'}$ gel phase. The DSPC bilayer is measured below the subtransition, pretransition, and transition temperatures (301, 324, and 328 K, respectively), which results in either an L_c stable crystalline phase or a metastable phase transitioning into it. The HSPC bilayer is a mixture of 11.4% DPPC and 88.6% DSPC, which means that there are two fractions, one of them being in the crystalline/metastable phase and the second one in the gel phase.[6,18] First, we used an experimental flicker noise spectroscopy, a measuring technique that links spontaneous bilayer fluctuations with its mechanical properties. The second technique was molecular dynamics (MD) simulations of small unilamellar vesicles. Due to its nature, it allows great insight into vesicle dynamics. To our knowledge, this is the first approach to measure an HSPC mixture using two different techniques.

EXPERIMENTAL METHODS AND PROCEDURES

Materials. Lipids DMPC (1,2-dimyristoyl-*sn*-glycero-3-phosphocholine), DSPC (1,2-distearoyl-*sn*-glycero-3-phosphocholine), DPPC (1,2-dipalmitoyl-*sn*-glycero-3-phosphocholine), and HSPC (L-α-phosphatidylcholine, mixture of 11.4% DPPC and 88.6% DSPC) were purchased from Avanti Polar Lipids (USA). The fluorescent probe Atto488-DOPE was purchased from Atto-Tech (Germany).

Preparation of Giant Unilamellar Vesicles (GUVs). A modified electroformation method was used to model the formation of lipid membranes.[19] Briefly, 20 μL of the chosen lipid in chloroform (3 mM) was deposited in small quantities (as 2 μL droplets) onto platinum electrodes. Two electrodes were set parallel to one another at a distance of 5 mm. The electrodes were kept for 1 h under reduced pressure to remove traces of organic solvents. Next, the electrodes were immersed in preheated pure aqueous solution. As we recently demonstrated,[20] a sufficient electroformation protocol consists of 4 h of electroformation with a 1 Hz AC electrical field applied in an electroformation chamber with the electrical field voltage set to 1 V for the first hour, 2 V for the second hour, 3 V for the third hour, and finally 4 V for the remaining time of the electroformation. In order to obtain GUVs from the investigated lipids, the temperature of the solvent was set at least 20 °C above the transition phase temperature of the investigated lipids (for example, it was 80 °C for HSPC). To this end, a custom glass electroformation chamber similar in design to thermal glasses combined with a heated bath (Lab. Companion RW-0525G, Poland) was used. After electroformation, the sample was left at the elevated temperature for an additional hour without the electrical field applied to allow the descent of the vesicles from the electrodes. Finally, the solution with GUVs was transferred to an unheated glass vial to induce a free decrease of solvent temperature to room temperature.

Acquisition and Assessment of Microscopic Images. The Cell Observer SD spinning disk confocal microscope (Zeiss, Germany) was used for vesicle recording. It was equipped with an α Plan-Apochromat 100×/1.46 oil immersion objective (Zeiss, Germany). 512 × 512 pixel images were recorded with an EMCCD camera (iXon3885, Andor, UK) using 2 × 2 binning with a 0.133 μm pixel size at a rate of 33 frames per second (fps) with a video integration time of 30 ms. At least 5000 images were recorded for each of the vesicles. Samples were illuminated with a 488 nm laser, and emitted light passed through the 527/54 filter. All samples were measured at 22 ± 1 °C (295 K). All measurements have been performed in a dedicated PTFE observation chamber with very limited height (equal to 300 μm) to reduce the effect of uncontrolled vesicle movements. The value of depth of focus was equal to 0.85 μm. To improve further quality of the analysis, the radius of the vesicle was calculated for each image, and when the fluctuations of the radius were unacceptable, as a result of misdetection caused by noise or other reasons described in previous work,[19] the image in the series was discarded from further analysis.

Flicker Noise Spectroscopy Analysis. The flicker noise spectroscopy technique is based on the analysis of vesicle shape fluctuations over time. In short, a membrane fluctuation spectrum was extracted from every single recorded image of the same lipid vesicle. This was performed using custom software.[19] To calculate the bending rigidity coefficient from a set of time-lapsed images, a correlation between the two-dimensional fluctuations and three-dimensional membrane elasticity model was established. This was

https://dx.doi.org/10.1021/acs.langmuir.0c00475
Langmuir 2020, 36, 3826−3835

achieved by calculating the angular autocorrelation function $\xi(\gamma, t)$ defined by eq 1. The cross-sectional radius $\rho(\Phi, t)$ is the position of the vesicle bilayer at a given angle Φ and time t; $\rho(t)$ is an averaged vesicle radius of a given image recorded at time t using eq 2. $R = \langle\rho(t)\rangle$ is the vesicle radius.

$$\xi(\gamma, t) = \frac{1}{2\pi^2 R^2}\int_0^{2\pi}[\rho(\phi+\gamma, t) - \rho(t)] \times [\rho(\phi, t) - \rho(t)]\,\mathrm{d}\phi \tag{1}$$

$$\rho(t) = \frac{1}{4\pi}\sum_{i=1}^{N}(\rho_i + \rho_{i+1}) \times (\phi_{i+1} - \phi_i) \tag{2}$$

The bending rigidity coefficient can be determined using two approaches, the statistical approach[19,21] and the averaged-based approach (AVB),[19,22] respectively. In the first one, autocorrelation curves are decomposed as cosine components of Fourier series. Since curves are even functions, sine components were not calculated. The amplitudes of cosine functions for each frame of a given mode m, $\chi^m(t)$, were next histogrammed and fitted by monoexponential distributions $\Gamma^m(\chi^m)$ according to eq 3.

$$\Gamma^m = a \times \exp\left(-R^m\left(\frac{\kappa}{kT}, \bar{\sigma}\right) \times \frac{\chi^m}{2}\right) \tag{3}$$

The monoexponential character of the distribution indicates that the model adequately describes the thermal fluctuations of the membrane. To bridge the bending rigidity coefficient with the obtained distributions, the decays were fitted using the monoexponential function for Γ^m ranging from 0.6 to 0.08. Higher values are omitted due to the low probability of the occurrence, while lower values were omitted due to being too close to the resolution limit. The uncertainty of the Γ^m value was calculated according to eq 4.

$$\Delta\Gamma^m = \frac{R^m}{\sqrt{N}} \times \sqrt{\sum_i\left(\ln\left[\Gamma^m\left(\frac{\chi_i^m}{2}\right)\right] - \ln(a) + R^m \times \frac{\chi_i^m}{2}\right)^2} \tag{4}$$

The bending rigidity coefficient can be determined by fitting eq 5 to the experimentally determined Γ^m values, where σ_{wh} is related to white noise generated by the limited optical resolution of the microscope and the electronic noise generated by the camera. $\mathcal{P}_n^m$ is the normalized Legendre polynomial, and $\lambda_n(\bar{\sigma})$ is the function related to the reduced membrane tension ($\bar{\sigma}$) defined by eq 6.

$$R^m\left(\frac{\kappa}{kT}, \bar{\sigma}, \sigma_{wh}\right) = \frac{1}{\frac{\kappa}{kT}\left(\sum_{n\geq m}^{n_{max}}\frac{[\mathcal{P}_n^m(0)]^2}{\lambda_n(\bar{\sigma})}\right) + {\sigma_{wh}}^2} \tag{5}$$

$$\lambda_n(\bar{\sigma}) = (n+1)(n+2)[\bar{\sigma} + n(n+1)] \tag{6}$$

In the average-based approach, angular autocorrelation curves (eq 1) are decomposed in the Legendre polynomial series. The decomposition is described by eq 7, where $B_n(t)$ with physical meaning (only positive values) is averaged over the position to obtain $\langle B_n\rangle$. Obtained $\langle B_n\rangle$ values are then plotted as a function of fluctuation mode number, and the bending rigidity coefficient is determined (eq 8). In the equation, k_B is the Boltzmann constant.

$$\xi(\gamma, t) = \langle B_0\rangle \times P_0(\cos\gamma) + \sum_{n=2}^{n_{max}} B_n(t) \times P_n(\cos\gamma) \tag{7}$$

$$\langle B_n\rangle \cong B_n(\kappa, \bar{\sigma}) = \frac{2n+1}{4\pi} \times \frac{k_B T}{\kappa(n+2)(n-1)[\bar{\sigma} + n(n+1)]} \quad \text{for } n > 1 \tag{8}$$

Molecular Dynamics Simulations. The full-atomistic molecular dynamics simulations were performed using NAMD 2.9[23] software with CHARMM36 united-atom force field[24] under NPT conditions (constant: number of particles, pressure, and temperature). The bending rigidity coefficient and area compressibility were determined for POPC, DMPC, DSPC, DPPC, and HSPC lipid vesicles. Each of the vesicles was modeled separately as a liposome with a 10 nm radius, and both sides were hydrated with TIP3P water molecules, giving a final simulation box of 30 nm^3. Three dimensional periodic boundary conditions were applied in order to deal with potential energy disruption due to the origin cell discontinuity. The vesicle system was created using a custom script in MATLAB. The starting area per lipid (APL) value was chosen to be 65.7 Å^2 for DPPC, 70 Å^2 for DMPC, 68.1 Å^2 for POPC, and 63.8 Å^2 for DSPC on average, respectively.[25] The APL was corrected to account for the effect of the vesicle's curvature by multiplying the APL value by 0.95 and 1.05 for inner and outer leaflets, respectively. This correction is a result of conclusions drawn by Braun and Sachs.[26] Vesicle systems, after the standard equilibration procedure, were subjected to at least the 10 ns production run and then analyzed. In order to determine a stable time point of equilibration, six selected parameters (mean values and standard deviations of both inner and outer leaflets, vesicle radius, and the thickness of the lipid bilayer) were continuously monitored. This was followed by determination of the order parameter drift. More detailed information regarding the setup of the systems and their properties are presented in Section 1 of the Supporting Information. Additionally, planar bilayers were simulated under the same conditions with 648 lipid molecules and a hydration level of 20 Å for comparison (details are presented in Section 4 of the Supporting Information).

Determination of Bending Rigidity Coefficient in MD. The bending rigidity of model lipid vesicles was determined according to the algorithm developed by Braun and Sachs.[26] It has an advantage over other approaches,[27] as it determines mechanical properties based on fluctuations of the bilayer within the vesicle. In short, each lipid is described by a vector spreading from the head (phosphorus atom) up to the tail position (midpoint of both 16th carbon atoms in each of the tails). This is followed by discrete surface representation θ, φ using a grid. For each time point, the surface of the fluctuations is established by the detection of the origin point of the fitted sphere, the conversion of the bilayer fluctuations into spherical coordinates, and the subtraction of the radius value. Finally, the average of both the inner and outer leaflet fluctuations is calculated. This is followed by spectral harmonics analysis (SPHA) for calculated fluctuations $f(\theta,\varphi)$. The fluctuations are represented as a linear combination of spherical harmonics with degree l and order m. Eventually, Helfrich's approach can be employed as described by eq 9, where a_{lm} is the spherical harmonic coefficient and Y_{lm} is the spherical harmonic basis function described by eq 10. The term $\tilde{P}_l^m$ defines the fully normalized associated Legendre polynomials.

$$f(\theta, \varphi) = \sum_{l,m} a_{lm} Y_{lm} \tag{9}$$

$$Y_{lm} = \tilde{P}_l^m(\cos\theta)e^{im\varphi} \tag{10}$$

In order to determine the values of the spherical harmonic coefficient, inverse transformation is used. To this end, matrix $\mathbf{P}$ for a given θ, φ distribution is generated, as presented in eq 11, where $l_i \in 0, \ldots, l_{max}$,

$$\mathbf{P}_{l_i}^{m} = \begin{bmatrix}\begin{pmatrix}\tilde{P}_0^m(\cos\theta_1) & \cdots & \tilde{P}_{l_i}^m(\cos\theta_1)\\ \vdots & \ddots & \vdots\\ \tilde{P}_0^m(\cos\theta_N) & \cdots & \tilde{P}_{l_i}^m(\cos\theta_N)\end{pmatrix}\end{bmatrix}^T \tag{11}$$

from which the matrix $\mathbf{Y}$ can be written as the spherical harmonic forward transformation (eq 12). In this equation, a_{lm}^1 is a recasting of spherical harmonic coefficients a_{lm} with dimensions corresponding to the row construction of $\mathbf{Y}$, and $f_{\theta,\varphi}^1$ is the matrix of the bilayer position.

$$\mathbf{Y}a_{lm}^1 = f_{\theta,\varphi}^1 \tag{12}$$

In order to calculate the inverse transformation (eq 13), the FACTORIZE package[28] in MATLAB was used. This allowed one to

https://dx.doi.org/10.1021/acs.langmuir.0c00475
Langmuir 2020, 36, 3826−3835

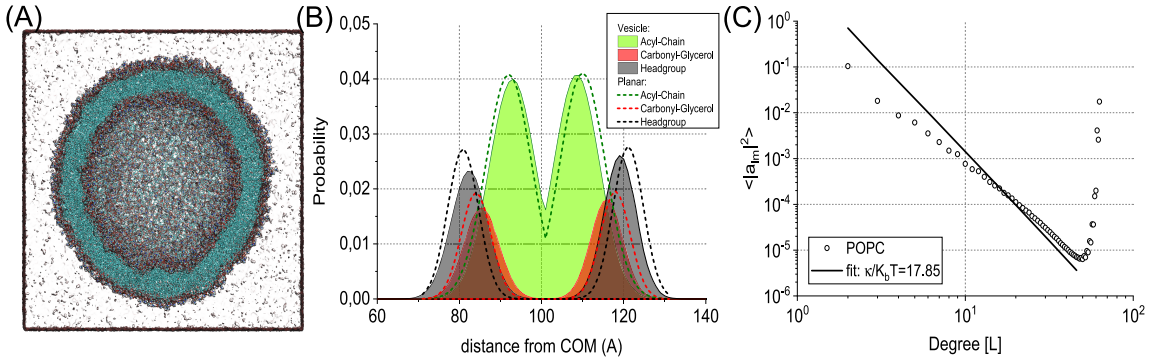

Figure 1. Molecular dynamics simulations of POPC membrane systems at 295 K. (A) A snapshot of the POPC vesicle cross-section in the water box. (B) Comparison of bilayer profiles for the POPC vesicle and the POPC planar system. (C) Undulation power spectra for the POPC vesicle system with the corresponding bending rigidity fit.

compute the approximation of the pseudoinverse of **Y** and apply it to determine a^1_{lm}.

$$\mathbf{Y}^{-1} f^1_{\theta,\varphi} = a^1_{lm} \tag{13}$$

From a^1_{lm}, the undulation power spectrum can be obtained by the binning modulus of the spherical harmonic coefficients across degree l. The resulting profile can be interpreted according to the Helfrich continuum model for undulations on a sphere with vanishing spontaneous curvature (eq 14), where T is temperature and k_B is the Boltzmann constant.

$$|a_{lm}|^2 = \frac{k_B T}{\kappa[l^2(l+1)^2 - 2l(l+1)]} \tag{14}$$

Determination of Basic Structural Parameters. Additional structural parameters were determined from MD simulations. Those include membrane thickness (MT), area per lipid (APL), and vesicle density profiles. For each frame, a sphere fit to the phosphorus atoms in the inner leaflet and in the outer leaflet and to all phosphorus atoms was done in order to obtain the radius for the inner leaflet, for the outer leaflet, and for the whole vesicle, respectively. MT was calculated as a difference between the radius of the outer and inner layers. APL, for the whole vesicle and each of the leaflets separately, was calculated according to eqs 15−17 as proposed by Braun and Sachs.[26]

$$\mathrm{ALP}_{\mathrm{vesicle}} = \frac{4\pi {r_{\mathrm{vesicle}}}^2}{\frac{1}{2}(n_{L,\mathrm{inner}} + n_{L,\mathrm{outer}})} \tag{15}$$

$$\mathrm{APL}_{\mathrm{inner}} = \frac{4\pi {r_{\mathrm{inner}}}^2}{n_{L,\mathrm{inner}}} \tag{16}$$

$$\mathrm{APL}_{\mathrm{outer}} = \frac{4\pi {r_{\mathrm{outer}}}^2}{n_{L,\mathrm{outer}}} \tag{17}$$

In order to determine the density vesicle profiles, three crucial zones of each vesicle in the lipid molecule particles were distinguished: headgroups, carbonyl−glycerol, and acyl chains. The vesicle center of mass is established with respect to all lipid molecule particles, which is followed by calculating the distance between particles and the established center of mass. This was done for at least the 100 last frames of the system. Eventually, the positions of the particles were histogrammed and fitted with a normal distribution.

Determination of Area Compressibility in Molecular Dynamics. In order to determine area compressibility (K_A), a method by Waheed and Edholm was used.[29] It allows one to separate the contributions from area fluctuations and undulations. First, the apparent area compressibility is calculated using eq 18, where A is the area of the system (calculated from the radius of the vesicle) and $\langle \delta A^2 \rangle$ is its mean square displacement.

$$K_A^{\mathrm{app}} = \frac{A \times k_B T}{\langle \delta A^2 \rangle} \tag{18}$$

Undulations and area changes in the curved surface occur independently of each other. The true value of area compressibility is determined using eq 19 for systems with low surface tension and eq 20 for systems with high surface tension.

$$\frac{1}{K_A^{\mathrm{true}}} = \frac{1}{K_A^{\mathrm{app}}} - \frac{A \times k_B T}{32\pi^3 \kappa^2} \tag{19}$$

$$\frac{1}{K_A^{\mathrm{true}}} = \frac{1}{K_A^{\mathrm{app}}} - \frac{A \times k_B T}{16.6\pi^3 \kappa^2} \tag{20}$$

RESULTS AND DISCUSSION

Validation of the Numerical Approach. In order to verify whether the numerical approach was correctly adapted, a well-characterized POPC lipid bilayer (TT = −2 °C, Figure 1A) was used as a reference.[5] The simulation system was equilibrated for 98 ns followed by an analysis time of 65 ns. Calculated membrane thickness (MT) was equal to 3.425 ± 0.008 nm. This result is slightly larger than in NMR experimental work, where it was equal to 3.05[30] or 2.98 nm.[31] On the other hand, the result was smaller than the membrane thickness (MT) obtained by X-ray scattering, which was equal to 3.9 ± 0.1 nm.[25] The calculated value of MT is also slightly smaller than the results from the MD studies of planar lipid bilayers ranging from 3.8[32] to 3.95 nm.[33] Since the result is within the range of reported values, it is considered correctly calculated.

The calculated area per lipid (APL) was equal to 57.7 ± 0.1 A^{o2} in the inner leaflet and 65.4 ± 0.1 A^{o2} in the outer leaflet. The APL calculated for the whole vesicle was equal to 61.4 ± 0.1 A^{o2}. Similar results were reported in the literature 40−65 A^{o2}.[27a,34]

The calculated vesicle density profile is presented in Figure 1B. For comparison, a profile calculated from the planar lipid bilayer is also included in the plot. While positions of the peaks representing membrane regions are similar for both systems, the distributions are different. In the planar system, the distributions are broader than these calculated for a vesicle. This indicates a higher mobility of lipids in a model system characterized by a lower curvature. This can be easily observed by looking at the peak of the carbonyl−glycerol groups (red dashed curve and red area in Figure 1B). In most experimental techniques, lipid vesicles are used as a model, for instance, to determine MT. Quantitative values of structural parameters

https://dx.doi.org/10.1021/acs.langmuir.0c00475
Langmuir 2020, 36, 3826−3835

calculated using the presented simulation model of the POPC vesicle are in good agreement with experimental data and simulations presented by others.

Finally, the bending rigidity coefficient was calculated and was equal to 7.40×10^{-20} J (which corresponds to $17.85\kappa/K_bT$ as shown in Figure 1C). This result is in good agreement with the bending rigidities obtained from other molecular dynamics studies.[27a,34] It was also within the limits of the reported experimental value based on the number of vesicles ($N = 10$) and equal to $(10.5 \pm 5.8) \times 10^{-20}$ J.[19] Calculated area compressibility (K_A) was equal to 0.23 N/m. Again, determined values for the vesicle model were in excellent agreement with other computational (0.24−0.28 N/m)[35] and experimental studies (0.18−0.33 N/m).[36] In summary, the presented computational approach delivers structural and mechanical data for the POPC (liquid) lipid bilayer, which is in good agreement with the results presented by others. Next, the computational approach combined with the experimental studies will be employed to characterize lipid bilayers in solid phases.

Basic Structural Properties. Table 1 presents calculated basic structural properties of the investigated solid-phase lipid vesicles. When one compares the results of APL obtained from vesicle simulations with literature data, significant differences in parameters can be observed.[25] In the investigated bilayers, it was determined that the APL for DPPC and DSPC systems is lower than for the corresponding measured experimental value by 20 and 17 Å^2, respectively. In the DMPC system, the value of the APL was in agreement with the membrane in the fluid phase. Additionally, this agreement was also confirmed by another MD simulation[26] and the experiment at 303 K.[37] Furthermore, for each of investigated vesicles, it was determined that the APL in the inner monolayer is higher than the one in the outer layer with the exception for DSPC and POPC systems. Such a difference was already reported in the literature. It was presumed by Braun and Sachs that its occurrence is caused by greater tension in the inner leaflet and tighter position distribution (as a result of unbalance in water density or lipid density across the vesicle).[26] Interestingly, during DMPC simulation, an occurrence of a spontaneous water pore was observed. It remained open until the balance of water densities inside and outside the lipid vesicle was reached, which has been followed by its closure. The observation is in good agreement with data presented by others.[38] Such an event can be explained by the fact that the DMPC membrane is in the rippled-gel phase, where the existence of interdigitated regions occurs. The starting points of the vesicle systems are lipids set opposite to each other. During the initial stages of simulation, an interdigitated region would need to emerge, which could result in high lateral pressure, resulting in spontaneous water pores and/or lack/excess of water to allow the appropriate confirmation for the interdigitated regions to emerge. Interestingly, a significant difference between the APL for the inner and outer layers was observed in the DMPC system. It was not observed in any other of the investigated systems. Hence, we believe that the difference is imposed by the system itself. Interestingly, the APL of the DMPC system is closer to the POPC system rather than the gel systems, which might suggest a high influence of the interdigitated regions in the rippled-gel phase. For liposomes consisting of lipids with high T_m (HSPC, DPPC, and DSPC), the determined APL was lower by about 20 Å^2 than that of the DMPC/POPC system. This well-known dependency[39] can be

Table 1. Summary of Calculated Parameters from a Molecular Dynamics (MD) Study and Flicker Noise Spectroscopy Measurements for Gel Phase Lipid Vesicles[a]

lipid type	membrane thickness [nm]	APL of vesicle [Å^2]	APL of inner membrane [Å^2]	APL of outer membrane [Å^2]	κ (MD, vesicle) [J]	κ (flicker, AVB) [J]	κ (flicker, SA) [J]	K_A (MD) [N/m]	κ (MD, planar) [J]
POPC	(3.425 ± 0.008)	(61.4 ± 0.1)	(57.7 ± 0.1)	(65.4 ± 0.1)	7.40×10^{-20}	$(10.5 \pm 2.2) \times 10^{-20}$	$(12 \pm 7) \times 10^{-20}$	0.23	$(10.8 \pm 0.3) \times 10^{-20}$
DMPC	(3.140 ± 0.007)	(60.5 ± 0.1)	(72.1 ± 0.1)	(56.3 ± 0.1)	7.22×10^{-20}	$(5.3 \pm 2.2) \times 10^{-20}$	$(6.0 \pm 2.0) \times 10^{-20}$	0.25	$(11.7 \pm 0.4) \times 10^{-20}$
DPPC	(4.059 ± 0.003)	(45.6 ± 0.1)	(47.2 ± 0.1)	(46.8 ± 0.1)	4.28×10^{-20}	$(5.0 \pm 3.3) \times 10^{-20}$	$(5.3 \pm 3.0) \times 10^{-20}$	0.31	$(23 \pm 1) \times 10^{-20}$
DSPC	(4.297 ± 0.004)	(46.8 ± 0.1)	(47.4 ± 0.1)	(48.5 ± 0.1)	3.74×10^{-20}	$(5.0 \pm 2.4) \times 10^{-20}$	$(4.5 \pm 2.6) \times 10^{-20}$	0.57	$(19.9 \pm 1.1) \times 10^{-20}$
HSPC	(4.290 ± 0.006)	(46.1 ± 0.1)	(45.6 ± 0.1)	(48.4 ± 0.1)	3.55×10^{-20}	$(3.5 \pm 1.8) \times 10^{-20}$	$(2.9 \pm 2.0) \times 10^{-20}$	0.26	$(23.2 \pm 1.8) \times 10^{-20}$

[a] APL, area per lipid; κ, bending rigidity coefficient; AVB, average-based approach; SA, statistical approach; K_A, true value of area compressibility.

https://dx.doi.org/10.1021/acs.langmuir.0c00475
Langmuir 2020, 36, 3826−3835

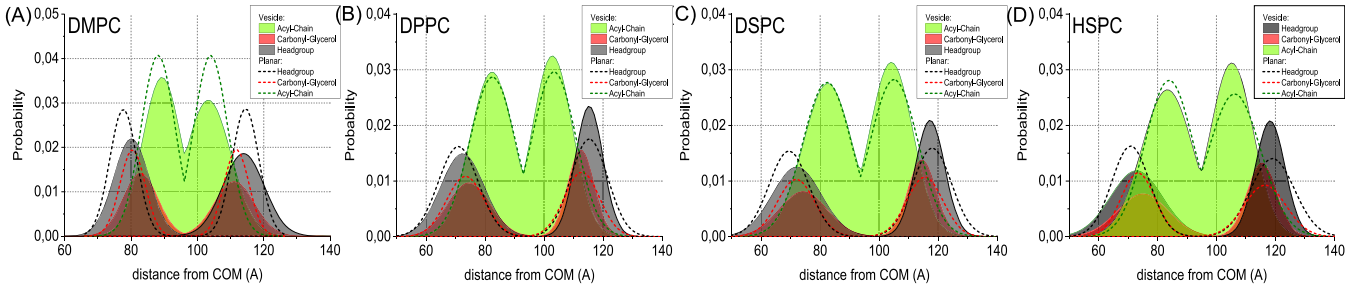

Figure 2. Comparison of component atom probabilities for (A) DMPC, (B) DPPC, (C) DSPC, and (D) HSPC lipid bilayers in molecular dynamics vesicle studies.

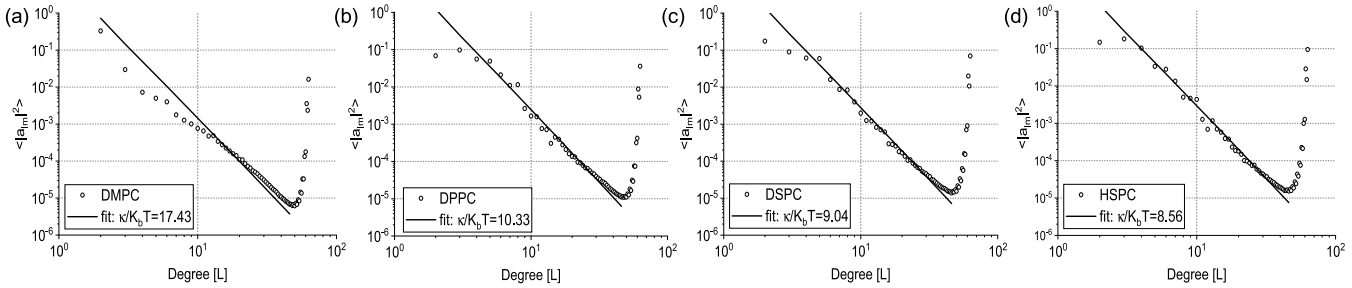

Figure 3. Fluctuations of the power spectra for (A) DMPC, (B) DPPC, (C) DSPC, and (D) HSPC vesicle systems with the corresponding bending rigidity (κ) fit.

explained by denser packing of lipid tails when the membrane is at a temperature substantially lower than the T_m. In the case of membrane thickness, a simple dependency is known: the higher the transition temperature of lipids, the higher is the membrane thickness of the bilayer.[39] Our results are in agreement with it. Similar conclusions can be drawn when analyzing density vesicle profiles in Figure 2. It can be observed that the main influence of the membrane thickness comes from the width of the acyl chain position population. The population width is smaller in DMPC, resulting in smaller MT contrary to other investigated bilayers. Furthermore, the profile does not change when the bilayer becomes heterogeneous as can be observed in the case of the HSPC bilayer. Profiles determined for the DSPC and DPPC lipids also remain the same in the case of the HSPC bilayer. All of the investigated vesicles sustained their quasi-spherical geometry.

Mechanical Parameters Determination. The bending rigidity coefficient was obtained using both computational and experimental approaches. The determined bending rigidity coefficients are presented in Table 1. The power spectra of the investigated lipid bilayers obtained using MD studies along with model fits are shown in Figure 3. Additionally, mechanical properties were determined for planar systems using the real-space fluctuation method (details are presented in Section 4 of the Supporting Information).

The value of the bending rigidity coefficient from the MD simulations for the DMPC lipid bilayer was equal to 7.22×10^{-20} J at 295 K. This value is slightly lower than the values for the DMPC bilayers obtained in our simulation of the flat-patch system (-1.2×10^{-19} J). The obtained values of the DMPC bending in the literature are for the bilayer in the liquid phase; however, they are presented to show the effect of the different phases. The obtained values for the ripple phase are lower than those reported in the literature for the liquid phase: -1.3×10^{-19} J for vesicle and 2.1×10^{-19} J for the flat-patch system (T = 303 K),[26] 1.45×10^{-19} J for the flat-patch system (T = 303 K),[40] and 1.22×10^{-19} J for the flat-patch system (T = 303 K).[35] Such a variation of the bending rigidity coefficient for the DMPC bilayers can be somewhat explained by the phase, topology, and/or water model. As reported in ref 41, the mechanical properties of the DMPC lipid bilayer, especially in gel/rippled phases, are very sensitive to temperature changes, especially when near T_m. A difference of 1 order of magnitude was reported in bending rigidity coefficient values of the DMPC lipid bilayer when changing the temperature from 293 to 296 K. It was shown that changes in the topology of the lipid bilayer influence the bending rigidity coefficient. For instance, vesicle systems tend to show generally smaller values compared to flat-patch systems in the MD simulation, although simulations were performed in the liquid phase (303 K).[26] It was also reported[26] that a small increase in the number of water molecules in the initial system can influence the obtained bending rigidity coefficient from 6.1×10^{-20} J up to 1.3×10^{-19} J for the DMPC system. Furthermore, as reported by Levine et al.,[27b] the value of the bending rigidity for another bilayer type, a DPPC bilayer, can differ significantly from 3.0×10^{-20} J up to 1.9×10^{-19} J, depending on the numerical approach used. All these factors can, in extreme cases, sum up to the difference of the magnitude in the value of the bending rigidity coefficient. Therefore, it is crucial to compare calculated values with experimental ones. According to the calculations, the area compressibility was equal to 0.25 N/m for the DMPC system. While this value is well within the range of values reported in the literature, a significant discrepancy in the literature can be found. The area compressibility for DMPC using the MD simulations was reported to be 0.25 N/m,[35] 0.23 N/m with a micropipette (temperatures not provided),[42] and decreased from 0.56 to 0.40 N/m with an increase of temperature from 300 up to 340 K with Neutron Spin Echo spectroscopy.[43]

In our MD simulations, the obtained value of the bending rigidity coefficient for the DPPC bilayer was equal to 4.28 ×

https://dx.doi.org/10.1021/acs.langmuir.0c00475
Langmuir 2020, 36, 3826−3835

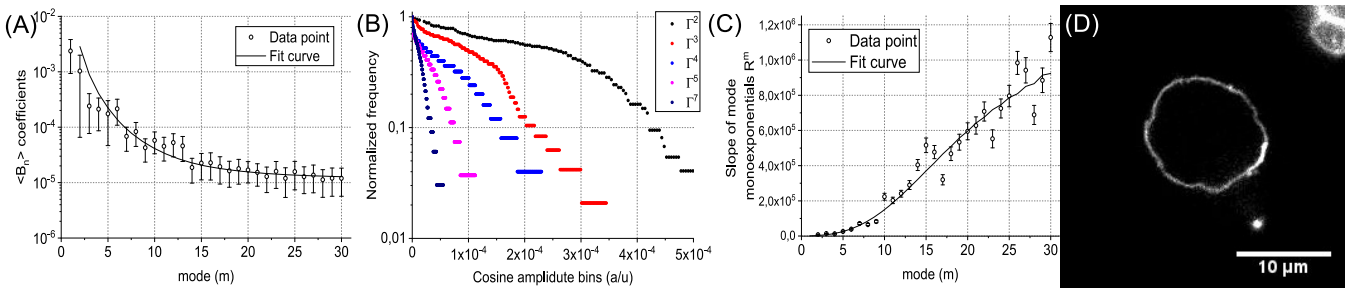

Figure 4. Flicker noise analysis of the HSPC vesicle. (A) Model fit of the $\langle B_n \rangle$ dependency on mode in the average-based approach. (B) Distribution Γ_m of shape fluctuations acquired by cosine decomposition in the statistical approach. (C) Model fit of slope R_m dependency on mode in the statistical approach. (D) Image of an HSPC vesicle with an oddly rectangular shape.

10^{-20} J at 295 K. This value is an order lower than the one we obtained for the flat-patch system (-2.3×10^{-19} J). Furthermore, this result differs by 1 order of magnitude from the values for the DPPC bilayer reported in the literature, which are 1.52×10^{-19} J for the flat-patch system (T = 303 K),[40] 1.56×10^{-18} J for the flat-patch system (T = 323 K),[27b] and 1.58×10^{-19} J for the flat-patch system (T = 323 K),[35] but we also found a much closer value to our finding of 4.52×10^{-20} J in the flat-patch system (T = 323 K).[44] It has to be noted that systems in the literature are above T_m; therefore, the comparison should be understood as an effect of phase change rather than a direct value comparison. Interestingly, the bending rigidity obtained for our flat-patch system is slightly higher than for those reported in the literature; however, this can also be explained by the phase difference. The area compressibility was equal to 0.31 N/m with our MD study. Similarly, the discrepancy can be observed with the area compressibility for DPPC equal to 0.21−0.23 N/m, depending on the size of the system in the MD studies,[35] 0.23 N/m with micropipette measurements (temperatures not provided),[42] and 0.56 N/m in 320 K with Neutron Spin Echo spectroscopy.[43]

Finally, bending rigidity coefficients for the DSPC and HSPC lipid bilayers obtained by the MD simulations were equal to 3.74×10^{-20} and 3.55×10^{-20} J, both at 295 K, respectively. Those values, yet again, were lower than the bending rigidities obtained in our flat-patch simulations. Those were equal to 2.0×10^{-19} and 2.3×10^{-19} J for DPSC and HSPC, respectively. No literature value for the bending rigidity coefficient was found for those bilayers. Area compressibility values were equal to 0.57 and 0.26 N/m for DSPC and HSPC lipid bilayers, respectively. Only the area compressibility for DSPC is available from the literature; it was reported to decrease from 0.50 down to 0.45 N/m with the temperature rising from 330 to 340 K using Neutron Spin Echo spectroscopy.[43] These results are consistent with ours since the temperature set in our simulations is 295 K. Therefore, the value of area compressibility should be higher, considering the dependence provided in the literature.

The calculated parameters were confronted with experimental values of the bending rigidity coefficient determined with the flicker noise technique. The experimental values presented in Table 1 are averaged over at least 10 vesicles. They are calculated using two different approaches: statistical and average-based (AVB) ones. An example of fluctuation distribution and model fits using both approaches is presented in Figure 4A−C. The details on individual measurements are presented in the Supporting Information in Section 3. Additionally, it should be noted that GUVs created from lipids with a T_m higher than room temperature tend to form oddly rectangular shapes rather than typical quasi-spherical ones. This is shown in Figure 4D and was not observed in our MD studies. The reason for this is probably due to the small size of the simulated vesicles and/or lack of the lipid bilayer rapid phase change in MD simulations.

Using flicker noise spectroscopy, the obtained values of the bending rigidity coefficient for the DMPC lipid bilayer using AVB and statistical approaches were equal to $(5.3 \pm 2.2) \times 10^{-20}$ and $(6.0 \pm 2.0) \times 10^{-20}$ J, both at 295 K, respectively. When compared to the literature, the values can be either within the range of error or even an order of magnitude higher, depending on the temperature, method, and data processing used. Using spin echo spectroscopy, the value of the bending rigidity coefficient for the DMPC bilayer was equal to 1.5×10^{-19} J at 300 K and 9.4×10^{-20} J at 340 K.[43] Using an optical dynamometry study, the value decreased from 2×10^{-18} to 4×10^{-20} J by increasing the temperature from 293 to 296 K.[41] Using flicker noise spectroscopy, the value was reported to be 1×10^{-19} J for 298 K.[45] Using the all-optical method, the value was equal to $(1.41 \pm 0.13) \times 10^{-19}$ J for 300 K and $(1.33 \pm 0.12) \times 10^{-19}$ J for 303 K,[46] respectively.

The experimentally determined bending rigidity coefficients for the DPPC lipid bilayer obtained with AVB and statistical approaches were equal to $(5.0 \pm 3.3) \times 10^{-20}$ and $(5.3 \pm 3.0) \times 10^{-20}$ J, both at 295 K, respectively. The measured value is lower than those reported with other experimental results. Specifically, with AFM indentation, the value of the bending rigidity coefficient for the DPPC bilayer was equal to 1.55×10^{-18} J for the vesicle system and 2.03×10^{-19} J for the supported lipid bilayer system at 293 K.[47] In another AFM study, the value was equal to $(1.3 \pm 0.1) \times 10^{-18}$ J.[48] Using spin echo spectroscopy, the value was equal to 2.08×10^{-19} J for 320 K.[43]

For the DSPC bilayer, the bending rigidity coefficient was equal to $(5.0 \pm 2.4) \times 10^{-20}$ and $(4.5 \pm 2.6) \times 10^{-20}$ J at 295 K using AVB and statistical approaches, respectively, in our study. Using spin echo spectroscopy, the value was equal to 2.28×10^{-19} J for 330 K.[43] There was no agreement between the results, probably due to the temperature difference.

Finally, for the HSPC bilayer, the values were equal to $(3.5 \pm 1.8) \times 10^{-20}$ and $(2.9 \pm 2.0) \times 10^{-20}$ J for 295 K using AVB and statistical approaches, respectively. No literature data regarding the bending rigidity of the HSPC bilayer is available.

It is well-known that different techniques yield inconsistent values for the bending rigidity coefficient.[49] Such discrepancies in the reported data are not surprising. On the other hand, the difference in the reported values of the bending rigidity between both vesicle simulation and flicker noise spectroscopy

https://dx.doi.org/10.1021/acs.langmuir.0c00475
Langmuir 2020, 36, 3826−3835

and both flat-patch simulations and the literature value is quite puzzling, especially given the fact that values of membrane thickness and APL are in agreement with the literature; additionally, there is an agreement for bending rigidity values between performed experimental calculations and simulations. It also should be noted that the obtained bending rigidity modulus from flicker noise spectroscopy compares very well with our theoretical simulations of the vesicles. When T_m of the investigated lipids is taken into account, an additional dependency can be found. It can be observed that the bending rigidity coefficient of the bilayers consisting of low T_m lipids are almost twice the value of bilayers consisting of lipids with higher T_m (difference between 7.22×10^{-20} and 3.55×10^{-20} J). This is, however, contrary to what we got when the bending rigidity was determined for flat-patch systems. This is also contrary to what one might expect, as a bilayer in the gel phase exhibits shear elasticity between individual lipid molecules and the effective energy required to bend the bilayer should be much higher than in the bilayers without it.[15] Another puzzling phenomena is the time constant deviation from the sphere shape observed in the vesicles, which bilayer is built from lipids with a high T_m, such as DPPC, DSPC, and HSPC (see Section 6 in the Supporting Information regarding the time stability of solid-ordered vesicles shapes). To this end, a different explanation is proposed, which could explain this discrepancy and phenomena. Since vesicles are formed by electroformation in high temperatures above T_m and then slowly cooled down, the phase-transition process is not rapid enough to cause the rupture of vesicles. What is happening is the slow stiffening of individual, small, flat patches, which rapidly meet at angles, slowly driven by the occurrence of another force, shear elasticity, which has been reported in bilayers below T_m. The system then is slowly reaching new minimal-energy configuration and, as result, the vesicle we are observing has a considerable deviation from sphericity. This would be extremely visible where the rigid flat patches meet. This would explain why, when analyzing the flat patch, the bending rigidity coefficient is very high, but when treating a system globally (as a vesicle), the system is hardly rigid at all. It would also explain the oddly rectangular shapes of the vesicles we were observing. It is also possible that these phenomena are observed only in a metastable phase, leading to the subgel phase of the membrane. However, this confirmation was observed for considerable amounts of time (at least hours), and the mechanical properties of the membrane in such a state are also worth investigating.

For area compressibility, the simple tendency in homogeneous lipid bilayers can be found; area compressibility increases with T_m. However, interesting phenomena can be observed in the case of heterogeneous HSPC. Despite both being a mixture of DPPC and DSPC and having a high T_m, its area compressibility is almost equal to that of DMPC (0.26 N/m) and is significantly lower than its component lipids. This result suggests that the heterogeneity of the lipid bilayers can influence the area compressibility in an unexpected nonlinear way.

SUMMARY AND CONCLUSIONS

In this paper, we have investigated the basic structure parameters (membrane thickness, area per lipid of both layers, and vesicle profiles) as well as mechanical properties (bending rigidity coefficient and area compressibility) of selected lipid bilayers. We have selected lipids on the basis of their transition temperature with an aim to investigate solid-ordered bilayers in physiological temperatures. To this end, lipids such as DMPC, DPPC, DSPC, and HSPC were chosen. Each of the bilayers built from those lipids are considered in different phases: rippled P_β gel phase, L_β gel phase, L_c stable crystalline or metastable phase, and the mixture of crystalline and gel phase lipids, respectively. Furthermore, POPC was chosen as a reference for the MD setup verification. Our results of area per lipid (APL) analysis confirmed that the parameter is lower for gel bilayers. We also reconfirmed that the higher value of membrane thickness is larger in solid-ordered than in liquid-ordered bilayers. Bending rigidity coefficients were determined using both flicker noise spectroscopy and 3D fluctuations spectra from MD studies. There was agreement in the parameters from experimental and computational techniques. For homogeneous bilayers, the bending rigidity coefficient decreased with an increase in the transition temperature of the lipids. These results are against intuition, as it could be argued that lipid bilayers are more resilient to mechanical stress when in the solid phase. Additionally, the obtained values of the bending rigidity coefficient were lower than in our flat-patch systems and in the literature data. Opposite dependencies were reported as well. We propose the explanation that the vesicle consists of rigid small patches. When analyzed locally, the bending rigidity is quite high, but when the system is analyzed globally, as for a vesicle, the value decreases, as individual small patches easily bend between each other. This view is additionally strengthened by the high deviation from sphericity observed in the investigated GUVs. Instead of the typical quasi-spherical shape, lipids with a higher T_m formed oddly rectangular shapes. This was mostly visible in HSPC and DSPC vesicles (crystalline phase or metastable phase), seen slightly less in DPPC (gel phase), and almost unobserved in DMPC (rippled gel phase). In the case of area compressibility, the parameter increased with T_m, suggesting that the presence of shear elasticity indeed limits stretching. Surprisingly, for the HSPC bilayer, the value of the bending rigidity was lower than both of its components and, at the same time, area compressibility was higher than both of its components. This suggests that the mechanical properties of the mixed bilayers cannot be straightforwardly calculated, due to either shear elasticity or the topology of the system. We hope that this work will prove valuable in further studies on solid-ordered bilayers as well as starting points to more detailed studies on the effect of bilayer topology from the mechanical point of view at the molecular level.

ASSOCIATED CONTENT

Supporting Information

The Supporting Information is available free of charge at https://pubs.acs.org/doi/10.1021/acs.langmuir.0c00475.

(1) Details of molecular dynamics simulations, (2) calculation of the order parameter for vesicle systems, (3) flicker noise analysis approach for molecular dynamics studies, (4) planar bilayer MD simulations details and mechanical parameters determination, (5) details of flicker noise measurements, and (6) time-stability of solid-ordered vesicles shapes (PDF)

https://dx.doi.org/10.1021/acs.langmuir.0c00475
Langmuir 2020, 36, 3826−3835

AUTHOR INFORMATION

Corresponding Author

Dominik Drabik − *Department of Biomedical Engineering, Faculty of Fundamental Problems of Technology, Wrocław University of Science and Technology, 50-377 Wrocław, Poland*; orcid.org/0000-0003-4568-4066; Email: Dominik.Drabik@pwr.edu.pl

Authors

Grzegorz Chodaczek − *PORT − Polish Center for Technology Development, 54-066 Wrocław, Poland*

Sebastian Kraszewski − *Department of Biomedical Engineering, Faculty of Fundamental Problems of Technology, Wrocław University of Science and Technology, 50-377 Wrocław, Poland*

Marek Langner − *Department of Biomedical Engineering, Faculty of Fundamental Problems of Technology, Wrocław University of Science and Technology, 50-377 Wrocław, Poland*

Complete contact information is available at: https://pubs.acs.org/10.1021/acs.langmuir.0c00475

Author Contributions

The manuscript was written through contributions of all authors. All authors have given approval to the final version of the manuscript.

Notes

The authors declare no competing financial interest.

ACKNOWLEDGMENTS

This work was possible thanks to the financial support from the National Science Centre (Poland) grant nos. 2016/21/N/NZ1/02767 and 2015/19/B/NZ7/02380 as well as statutory funds from Wroclaw University of Technology. Numerical resources for Molecular Dynamics simulations were granted by Wroclaw Centre of Networking and Supercomputing, grant no. 274.

ABBREVIATIONS

T_m, transition temperature; MD, molecular dynamics; AVB, averaged-based approach; APL, area per lipid; SPHA, spherical harmonics analysis; MT, membrane thickness

REFERENCES

(1) Stillwell, W. Introduction to Biological Membranes. In *An Introduction to Biological Membranes*; Gonzalez, P., Ed.; Elsevier: United Kingdom, 2013; pp 3−6.

(2) Humphrey, J. D.; Dufresne, E. R.; Schwartz, M. A. Mechanotransduction and extracellular matrix homeostasis. *Nat. Rev. Mol. Cell Biol.* **2014**, *15* (12), 802−12.

(3) Alonso, M. A.; Millan, J. The role of lipid rafts in signalling and membrane trafficking in T lymphocytes. *J. Cell Sci.* **2001**, *114*, 2957−2965.

(4) Milhaud, J. New insights into water−phospholipid model membrane interactions. *Biochim. Biophys. Acta, Biomembr.* **2004**, *1663* (1−2), 19−51.

(5) Dimova, R. Recent developments in the field of bending rigidity measurements on membranes. *Adv. Colloid Interface Sci.* **2014**, *208*, 225−234.

(6) Marsh, D. Phase Transition Temperatures. In *Handbook of lipid bilayers*; Taylor & Francis Group: New York, 2013; pp 539−600.

(7) (a) Nagle, J. F. Theory of the main bilayer phase transition. *Annu. Rev. Phys. Chem.* **1980**, *31*, 157−195. (b) Bagatolli, L.; Sunil Kumar, P. B. Phase behavior of multicomponent membranes: Experimental andcomputational techniques. *Soft Matter* **2009**, *5*, 3234−3248.

(8) (a) Melchior, D. L. Lipid domains in fluid membranes: a quick-freeze differential scanning calorimetry study. *Science* **1986**, *234* (4783), 1577−80. (b) Lentz, B. R.; Barenholz, Y.; Thompson, T. E. Fluorescence depolarization studies of phase transitions and fluidity in phospholipid bilayers. 2. Two-component phosphatidylcholine liposomes. *Biochemistry* **1976**, *15* (20), 4529−4537. (c) Mabrey, S.; Sturtevant, J. M. Investigation of phase transitions of lipids and lipid mixtures by sensitivity differential scanning calorimetry. *Proc. Natl. Acad. Sci. U. S. A.* **1976**, *73* (11), 3862−3866.

(9) Jørgensen, K.; Sperotto, M. M.; Mouritsen, O. G.; Ipsen, J. H.; Zuckermann, M. J. Phase equilibria and local structure in binary lipid bilayers. *Biochim. Biophys. Acta, Biomembr.* **1993**, *1152* (1), 135−145.

(10) (a) Ruocco, M. J.; Shipley, G. G. Interaction of cholesterol with galactocerebroside and galactocerebroside-phosphatidylcholine bilayer membranes. *Biophys. J.* **1984**, *46* (6), 695−707. (b) Norlen, L. Skin barrier structure and function: the single gel phase model. *J. Invest. Dermatol.* **2001**, *117* (4), 830−836.

(11) Jouhet, J. Importance of the hexagonal lipid phase in biological membrane organization. *Front. Plant Sci.* **2013**, *4*, 494.

(12) Yi, X.; Gao, H. Kinetics of receptor-mediated endocytosis of elastic nanoparticles. *Nanoscale* **2017**, *9* (1), 454−463.

(13) (a) Ishida, T.; Harashima, H.; Kiwada, H. Liposome clearance. *Biosci. Rep.* **2002**, *22* (2), 197−224. (b) Moghimi, S. M.; Hunter, A. C.; Murray, J. C. Long-circulating and target-specific nanoparticles: theory to practice. *Pharmacol. Rev.* **2001**, *53* (2), 283−318. (c) Lombardo, D.; Calandra, P.; Barreca, D.; Magazu, S.; Kiselev, M. A. Soft Interaction in Liposome Nanocarriers for Therapeutic Drug Delivery. *Nanomaterials* **2016**, *6* (7), 125.

(14) Bouvrais, H.; Holmstrup, M.; Westh, P.; Ipsen, J. H. Analysis of the shape fluctuations of reconstitued membranes using GUVs made from lipid extracts of invertebrates. *Biol. Open* **2013**, *2*, 373−378.

(15) Helfrich, W. Elastic Properties of Lipid Bilayers: Theory and Possible Experiments. *Z. Naturforsch., C: J. Biosci.* **1973**, *28* (c), 693−703.

(16) Brochard, F.; Lennon, J. F. Frequency Spectrum of the Flicker Phenomenon in Erythrocytes. *J. Phys. (Paris)* **1975**, *36* (11), 1035−1047.

(17) Akabori, K.; Nagle, J. F. Structure of the DMPC lipid bilayer ripple phase. *Soft Matter* **2015**, *11* (5), 918−26.

(18) (a) Silvius, J. R. *Thermotropic Phase Transitions of Pure Lipids in Model Membranes and Their Modifications by Membrane Proteins*; John Wiley & Sons, Inc.: New York, 1982. (b) Lewis, R. N. A. H.; Mak, N.; McElhaney, R. N. A differential scanning calorimetric study of the thermotropic phase behavior of model membranes composed of phosphatidylcholines containing linear saturated fatty acyl chains. *Biochemistry* **1987**, *26* (19), 6118−6126.

(19) Drabik, D.; Przybyło, M.; Chodaczek, G.; Iglič, A.; Langner, M. The modified fluorescence based vesicle fluctuation spectroscopy technique for determination of lipid bilayer bending properties. *Biochim. Biophys. Acta, Biomembr.* **2016**, *1858* (2), 244−252.

(20) Drabik, D.; Doskocz, J.; Przybyło, M. Effects of electroformation protocol parameters on quality of homogeneous GUV populations. *Chem. Phys. Lipids* **2018**, *212*, 88−95.

(21) Meleard, P.; Pott, T.; Bouvrais, H.; Ipsen, J. H. Advantages of statistical analysis of giant vesicle flickering for bending elasticity measurements. *Eur. Phys. J. E: Soft Matter Biol. Phys.* **2011**, *34*, 116.

(22) Pecreaux, J.; Döbereiner, H.-G.; Prost, J.; Joanny, J.-F.; Bassereau, P. Refined contour analysis of giant unilamellar vesicles. *Eur. Phys. J. E: Soft Matter Biol. Phys.* **2004**, *13*, 277−290.

(23) Phillips, J. C.; Braun, R.; Wang, W.; Gumbart, J.; Tajkhorshid, E.; Villa, E.; Chipot, C.; Skeel, R. D.; Kale, L.; Schulten, K. Scalable molecular dynamics with NAMD. *J. Comput. Chem.* **2005**, *26* (16), 1781−1802.

(24) Lee, S.; Tran, A.; Allsopp, M.; Lim, J. B.; Hénin, J.; Klauda, J. B. CHARMM36 United Atom Chain Model for Lipids and Surfactants. *J. Phys. Chem. B* **2014**, *118* (2), 547−556.

(25) Kučerka, N.; Nieh, M.-P.; Katsaras, J. Fluid phase lipid areas and bilayer thicknesses of commonly used phosphatidylcholines as a

function of temperature. *Biochim. Biophys. Acta, Biomembr.* **2011**, *1808*, 2761−2771.
(26) Braun, A. R.; Sachs, J. N. Determining Structural and Mechanical Properties from Molecular Dynamics Simulations of Lipid Vesicles. *J. Chem. Theory Comput.* **2014**, *10*, 4160−4168.
(27) (a) Khelashvili, G.; Johner, N.; Zhao, G.; Harries, D.; Scott, H. L. Molecular origins of bending rigidity in lipids with isolated and conjugated double bonds: The effect of cholesterol. *Chem. Phys. Lipids* **2014**, *178*, 18−26. (b) Levine, Z. A.; Venable, R. M.; Watson, M. C.; Lerner, M. G.; Shea, J.-E.; Pastor, R. W.; Brown, F. L. H. Determination of Biomembrane Bending Moduli in Fully Atomistic Simulations. *J. Am. Chem. Soc.* **2014**, *136*, 13582−13585. (c) Kawamoto, S.; Nakamura, T.; Nielsen, S. O.; Shinoda, W. A guiding potential method for evaluating the bending rigidity of tensionless lipid membranes from molecular simulation. *J. Chem. Phys.* **2013**, *139*, No. 034108.
(28) Davies, T. A. Algorithm 930: FACTORIZE: An object-oriented linear system solver for MATLAB. *ACM Transactions on Mathematical Software* **2013**, *39* (4), 28.
(29) Waheed, Q.; Edholm, O. Undulation Contributions to the Area Compressibility in Lipid Bilayer Simulations. *Biophys. J.* **2009**, *97*, 2754−2760.
(30) Harzer, U.; Bechinger, B. Alignment of Lysine-Anchored Membrane Peptides under Conditions of Hydrophobic Mismatch: A CD, ^{15}N and ^{31}P Solid-State NMR Spectroscopy Investigation. *Biochemistry* **2000**, *39*, 13106−13114.
(31) Nezil, F. A.; Bloom, M. Combined influence of cholesterol and synthetic amphiphillic peptides upon bilayer thickness in model membranes. *Biophys. J.* **1992**, *61*, 1176−1183.
(32) Pasenkiewicz-Gierula, M; Murzyn, K; Rog, T; Czaplewski, C Molecular dynamics simulation studies of lipid bilayer systems. *Acta Biochimica Polonica* **2000**, *47*, 601−611.
(33) Tsai, H.-H. G.; Lee, J.-B.; Huang, J.-M.; Juwita, R. A Molecular Dynamics Study of the Structural and Dynamical Properties of Putative Arsenic Substituted Lipid Bilayers. *Int. J. Mol. Sci.* **2013**, *14*, 7702−7715.
(34) MacDermaid, C. M.; Kashyap, H. K.; DeVane, R. H.; Shinoda, W.; Klauda, J. B.; Klein, M. L.; Fiorin, G. Molecular dynamics simulations of cholesterol-rich membranes using a coarsegrained force field for cyclic alkanes. *J. Chem. Phys.* **2015**, *143*, 243144.
(35) Venable, R. M.; Brown, F. L. H.; Pastor, R. W. Mechanical properties of lipid bilayers from molecular dynamics simulation. *Chem. Phys. Lipids* **2015**, *192*, 60−74.
(36) Nagle, J. F.; Tristram-Nagle, S. Structure of lipid bilayers. *Biochim. Biophys. Acta, Rev. Biomembr.* **2000**, *1469* (3), 159−195.
(37) Petrache, H. I.; Dodd, S. W.; Brown, M. F. Area per lipid and acyl length distributions in fluid phosphatidylcholines determined by (2)H NMR spectroscopy. *Biophys. J.* **2000**, *79* (6), 3172−92.
(38) Lis, M.; Wizert, A.; Przybylo, M.; Langner, M.; Swiatek, J.; Jungwirth, P.; Cwiklik, L. The effect of lipid oxidation on the water permeability of phospholipids bilayers. *Phys. Chem. Chem. Phys.* **2011**, *13* (39), 17555−63.
(39) Kinnun, J. J.; Mallikarjunaiah, K. J.; Petrache, H. I.; Brown, M. F. Elastic deformation and area per lipid of membranes: atomistic view from solid-state deuterium NMR spectroscopy. *Biochim. Biophys. Acta, Biomembr.* **2015**, *1848* (1 Pt B), 246−259.
(40) Doktorova, M.; Harries, D.; Khelashvili, G. Determination of bending rigidity and tilt modulus of lipid membranes from real-space fluctuation analysis of molecular dynamics simulations. *Phys. Chem. Chem. Phys.* **2017**, *19*, 16806.
(41) Dimova, R.; Pouligny, B.; Dietrich, C. Pretransitional Effects in Dimyristoylphosphatidylcholine Vesicle Membranes: Optical Dynamometry Study. *Biophys. J.* **2000**, *79* (1), 340−356.
(42) Rawicz, W.; Olbrich, K. C.; McIntosh, T.; Needham, D.; Evans, E. Effect of chain length and unsaturation on elasticity of lipid bilayers. *Biophys. J.* **2000**, *79* (1), 328−39.
(43) Nagao, M.; Kelley, E. G.; Ashkar, R.; Bradbury, R. D.; Butler, P. D. Probing Elastic and Viscous Properties of Phospholipid Bilayers Using Neutron Spin Echo Spectroscopy. *J. Phys. Chem. Lett.* **2017**, *8* (19), 4679−4684.
(44) Hofsäß, C.; Lindahl, E.; Edholm, O. Molecular Dynamics Simulations of Phospholipid Bilayers with Cholesterol. *Biophys. J.* **2003**, *84* (4), 2192−2206.
(45) Meleard, P.; Gerbeaud, C.; Pott, T.; Fernandez-Puente, L.; Bivas, I.; Mitov, M. D.; Dufourcq, J.; Bothorel, P. Bending Elasticities of Model Membranes: Influences of Temperature and Sterol Content. *Biophys. J.* **1997**, *72*, 2616−2629.
(46) Lee, C.-H.; Lin, W.-C.; Wang, J. All-optical measurements of the bending rigidity of lipid-vesicle membranes across structural phase transitions. *Phys. Rev. E: Stat. Phys., Plasmas, Fluids, Relat. Interdiscip. Top.* **2001**, *64*, No. 020901(R).
(47) Et-Thakafy, O.; Delorme, N.; Gaillard, C.; Mériadec, C.; Artzner, F.; Lopez, C.; Guyomarc'h, F. Mechanical properties of membranes composed of gel-phase or fluid-phase phospholipids probed on liposomes by atomic force spectroscopy. *Langmuir* **2017**, *33* (21), 5117−5126.
(48) Delorme, N.; Fery, A. Direct method to study membrane rigidity of small vesicles basedon atomic force microscope force spectroscopy. *Phys. Rev. E* **2006**, *74*, No. 030901(R).
(49) Nagle, J. F. Introductory Lecture: Basic quantities in model biomembranes. *Faraday Discuss.* **2013**, *161*, 11−29.

https://dx.doi.org/10.1021/acs.langmuir.0c00475
Langmuir 2020, 36, 3826−3835